

# Pumped Thermal Grid Storage with Heat Exchange

Robert B. Laughlin

Department of Physics, Stanford University, Stanford, CA 94305\*

(Dated: February 5, 2016)

A thermal heat-pump grid storage technology is described based on closed-cycle brayton engine transfers of heat from a cryogenic storage fluid to molten solar salt. Round-trip efficiency is computed as a function of turbomachinery polytropic efficiency and total heat exchanger steel mass and is found to be competitive with that of pumped hydroelectric storage. The cost per engine watt and cost per stored joule based is estimated based on the present-day prices of power gas turbines and market prices of steel and nitrate salt. Comparison is made with electrochemical and mechanical grid storage technologies.

## I. INTRODUCTION

It is widely understood that facilities for storing very large amounts electric energy are key to any long-term plan to supplant fossil fuel with renewable energy.<sup>1-3</sup> The desirability of switching to renewable sources is, of course, controversial, and it is not clear that eliminating fossil fuel is economically feasible at this time.<sup>4-7</sup> But without storage it is also impossible.<sup>8</sup> The intermittencies of energy sources like the wind and sun are fundamentally incompatible with the electricity industry's need to supply power to customers the instant customer demands. The overriding importance of timing is demonstrated by the frequent development of negative spot prices for electric energy in markets with large wind deployments.<sup>9-12</sup>

The purpose of this paper is to discuss a specific storage technology and make the case that it is has the right engineering compromises to prevail when the need for storage eventually becomes acute. It is a version of pumped thermal storage, an idea already in the literature and under development industrially, and differs from it chiefly in the substitution for heat exchangers for thermoclines.<sup>13-17</sup> It is illustrated in Fig. 1. Instead of pumping water uphill from a low reservoir to a higher one to store energy, as occurs in pumped hydroelectricity, one pumps heat from a cold body to a hot one by means of a heat engine. In either case the process is reversible, so that energy banked can be withdrawn later to satisfy demand.

The reasoning leading to the “brayton battery”, as it might be called, applies the metrics of safety, low cost, and high efficiency, *in that order*. The average power delivered to a large metropolitan area such as Los Angeles or New York is about  $1.4 \times 10^{10}$  watts.<sup>18</sup> Storing this power for only one hour gives  $5.04 \times 10^{13}$  joules, or one Hiroshima-sized atomic bomb.<sup>19</sup> It is absolutely essential that explosive release of this stored energy be physically impossible. Once this safety criterion is met, capital and maintenance costs must be brutally minimized, even at the price of a small hit in round-trip efficiency, because storage of electricity is fundamentally about value, not about conserving energy.

The round-trip storage efficiency  $\eta_{store}$  of the configuration in Fig. 1 satisfies

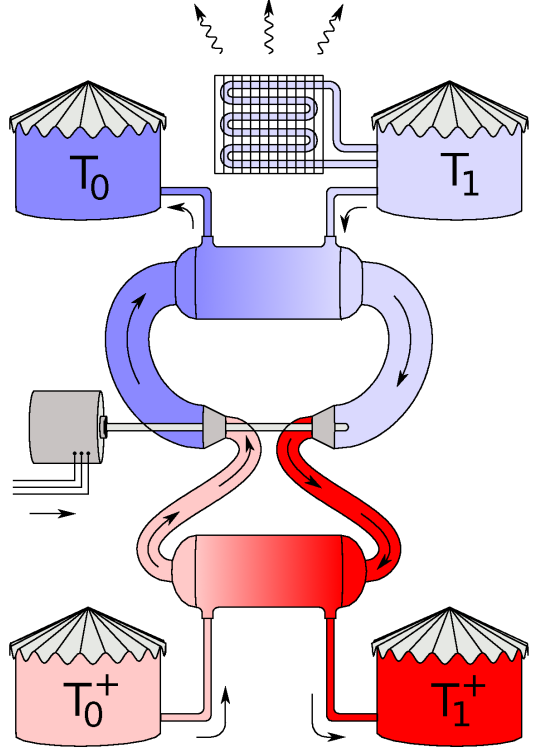


FIG. 1: Conceptual diagram of pumped thermal storage with heat exchange. Heat is added/removed from the working fluid of a closed-cycle brayton engine by means of heat exchangers with counterflowing storage fluids. The latter are stored in four tanks at different temperatures constrained by the condition  $T_0^+/T_0 = T_1^+/T_1 = \xi$ . In the limit that the turbine-compressor pair is perfectly adiabatic and the heat exchangers are very large, the engine is fully reversible. Nonideality in both the turbomachinery and the heat exchangers generates entropy that must be sloughed into the environment as waste heat.

$$\eta_{store} < 1 - \frac{2T_{dump}}{T_1 - T_0} \left( \frac{1}{\eta_c} - \eta_t \right) \frac{\ln(\xi)}{\xi - 1} \quad (1)$$

where  $\eta_c$  and  $\eta_t$  are the polytropic efficiencies of the compressor and turbine, respectively, and  $T_{dump}$  is the

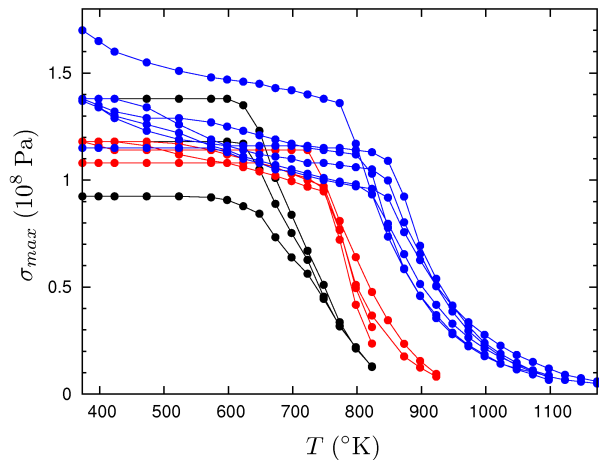


FIG. 2: Maximum steel stress allowed by the 2007 ASME Boiler and Pressure Vessel Code, Part II, Section D, Tables 1A and 1B for a representative selection of steels (seamless tubing).<sup>22</sup> The “creep cliff” at  $T = 873^\circ\text{K}$  ( $600^\circ\text{C}$ ) is clearly visible. Black: Carbon steels, UNS Nos. K01201, K02707, and K03501. Red: Low-alloy steels, UNS Nos. K11522, K11547, K11597, and K21590. Blue: Stainless steels, UNS Nos. S30409, S30815, S31609, S32109, S34709, and N08810 (Incalloy 800H).

(Kelvin) temperature at which waste heat is sloughed. For the prototype parameters in Table I), this limit is 0.75. The factor of two in Eqn. (1), which comes from the need to pass the working fluid through the turbomachinery twice in each storage cycle, is the efficiency disadvantage vis-a-vis pumped hydroelectricity or thermoclines.

The plan of the paper is as follows. Section II discusses materials, with emphasis on the properties of steels and storage fluids and the constraints these impose on operating temperatures. Section III deals with regeneration, the need for which follows from the materials constraints. Section IV is a detailed round-trip efficiency computation. Section V discusses costs. Section VI is a summary.

## II. MATERIALS

### A. Steel Limitations

Closing the brayton cycle as shown in Fig. 1 enables the background working fluid pressure to be raised, thus greatly reducing the cost per engine watt. The turbine rotation speed and blade angles fix the working fluid velocity to first approximation, so increasing the pressure simply increases the number of moles of working fluid passing a given point per second and thus the total power. Background pressures as high as  $7.7 \times 10^6$  Pa (77 atmospheres) compressed to to  $1.38 \times 10^7$  Pa have been experimentally benchmarked in closed-cycle brayton engines using supercritical  $\text{CO}_2$ .<sup>20</sup> Pressures approaching

	Ar	$\text{N}_2$
$T_0$	$180^\circ\text{K}$	$180^\circ\text{K}$
$T_0^+$	$300^\circ\text{K}$	$300^\circ\text{K}$
$T_1$	$495^\circ\text{K}$	$495^\circ\text{K}$
$T_1^+$	$823^\circ\text{K}$	$823^\circ\text{K}$
$T_{dump}$	$300^\circ\text{K}$	$300^\circ\text{K}$
$\xi$	1.66	1.66
$\eta_c$	0.91	0.91
$\eta_t$	0.93	0.93
$p_0$	$1.00 \times 10^5$ Pa	$1.00 \times 10^5$ Pa
$p_l$	$1.00 \times 10^6$ Pa	$1.00 \times 10^6$ Pa
$p_h$	$3.55 \times 10^6$ Pa	$6.52 \times 10^5$ Pa

TABLE I: Prototype design parameters assumed throughout this paper. The differences between charge and discharge are ignored for clarity, as is the need to make  $T_{dump}$  higher than ambient to slough heat effectively. The compressor polytropic efficiency  $\eta_c$  is the ratio of ideal compressive work to actual work in the limit of small compression (*i.e.* for a single stage). The turbine polytropic efficiency  $\eta_t$  is the inverse of this ratio in the limit of small expansion. These particular values  $\eta_c$  and  $\eta_t$  are industry standards discussed further in Section IV B.<sup>59–63</sup>

$3.0 \times 10^7$  Pa (300 atmospheres) are routine in modern supercritical steam power plants.<sup>21</sup>

However, the use of high pressure severely limits the temperatures one can employ. As shown in Fig. 2, raising the temperature of a steel eventually causes it to exhibit creep, a slow plastic deformation that presages full mechanical failure at higher temperatures. This effect is irrelevant on short time scales but is a major design constraint on the scale of 40 years.<sup>22</sup> Creep is what prevents conventional carbon steels from being used in high-pressure thermal applications at temperatures above about  $700^\circ\text{K}$  ( $427^\circ\text{C}$ ). This limit can be raised to about  $800^\circ\text{K}$  ( $527^\circ\text{C}$ ) by adding impurities in percent amounts that block grain boundary motion, but maximum resistance to creep requires fully alloying with Cr and Ni to make stainless steels.<sup>22</sup> The creep limitations of alloy steels may be seen from Fig. 2 to apply universally, including to Inconels. Thus pressure vessels constructed from steel become problematic for temperatures much above  $873^\circ\text{K}$  ( $600^\circ\text{C}$ ). This is a major consideration in present-day supercritical steam plants.<sup>21</sup>

### B. Solar Salt

The temperature limitations of steels cause solar salt, the elementary  $\text{NaNO}_3/\text{KNO}_3$  eutectic storage medium of the concentrating solar industry, to be a particularly good choice for the high-temperature storage medium.<sup>23–25</sup> All solid and liquid substances have heat capacities of approximately  $3R$  per mole of atoms, where  $R$  is the ideal gas constant, in the temperature range of interest, so virtually anything will do as thermal stor-

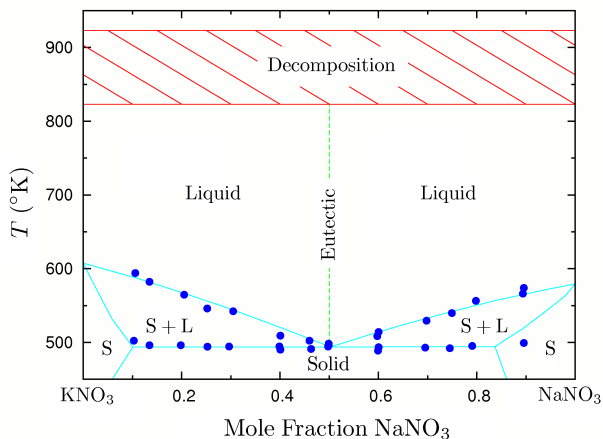


FIG. 3: The  $\text{NaNO}_3/\text{KNO}_3$  phase diagram, after Rogers and Janz.<sup>26</sup> The measurements of the liquidus and solidus lines are from Rogers and Janz and also Kramer and Wilson<sup>27</sup>. The lines are theory due to Zhang *et al.*<sup>28</sup> The eutectic freezing temperature is  $495^\circ\text{K}$  ( $222^\circ\text{C}$ ). The decomposition temperature is  $823^\circ\text{K}$  ( $550^\circ\text{C}$ ).<sup>29–32</sup>

age medium, including rocks. However, the cost of either gravel or salt is much less than the cost of the engine for storage times less than 1 day, and salt has the great advantage of being liquid and thus enabling heat transfer by counterflow, minimizing entropy creation. Solar salt has a well-known list of other advantages such as low vapor pressure, high compatibility with steels, and environmental friendliness. It does not disintegrate in response to thermal cycling stresses the way a solid would. It creates no explosion hazard.

The  $\text{NaNO}_3/\text{KNO}_3$  phase diagram is shown in Fig. 3.<sup>26–28</sup> At the eutectic composition (0.5 molar fraction of  $\text{NaNO}_3$ ) the melting temperature is  $495^\circ\text{K}$  ( $220^\circ\text{C}$ ), about the same as ordinary Pb/Sn solder. There is also decomposition boundary at approximately  $823^\circ\text{K}$  ( $550^\circ\text{C}$ ), a temperature conveniently near the steel creep cliff seen in Fig. 1.<sup>29–32</sup> The decomposition boundary is the point where performance becomes difficult to predict, not where the salt begins to fail. The first stages of  $\text{NO}_3$  decomposition are reversible and occur via the nitrate/nitrite reaction  $2\text{NO}_3^- \rightarrow 2\text{NO}_2^- + \text{O}_2$ . Approximately 3% of the nitrate has converted to nitrite at  $823^\circ\text{K}$  ( $550^\circ\text{C}$ ).<sup>29</sup> The kinetics of outgassing and re-absorption of  $\text{O}_2$  have been measured and found not to be unduly rapid.<sup>30,31</sup> Nitrogen oxide and  $\text{N}_2$  evolve irreversibly at high rates above  $923^\circ\text{K}$  ( $700^\circ\text{C}$ ).<sup>32</sup> The true upper operating temperature of solar salt exposed to air is not presently known.<sup>32</sup> The corrosion of stainless steels by these salts is mild and amounts to approximately  $10 \mu\text{m}$  per year at  $823^\circ\text{K}$  ( $550^\circ\text{C}$ ), chiefly due to oxidation.<sup>33,34</sup>

Fig. 4 shows the important thermophysical properties of solar salt over the temperature range of interest.<sup>35–37</sup>

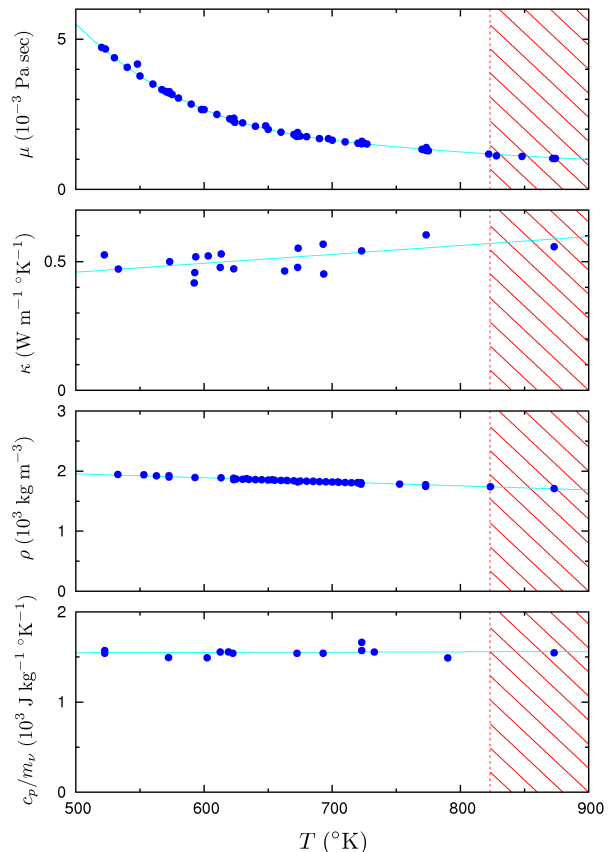


FIG. 4: Thermophysical properties of  $\text{NaNO}_3/\text{KNO}_3$  eutectic. The viscosity data are from from Janz *et al.* as supplemented by Lasfargues *et al.*<sup>35,36</sup> The solid line is the fit of Janz *et al.* splined at  $730^\circ\text{K}$  to a power series in  $1/T$ . The remaining data and the interpolations through them are from Bauer *et al.*<sup>37</sup> The molar mass per formula unit is  $m_\nu = 0.094 \text{ kg mol}^{-1}$ . The equipartition heat capacity is  $c_p^{\text{ideal}}/m_\nu = 15R/m_\nu = 1330 \text{ J }^\circ\text{K}^{-1} \text{ kg}^{-1}$ . For comparison, room-temperature water has  $\mu = 0.001 \text{ Pa sec}$ ,  $\kappa = 0.59 \text{ W m}^{-1} \text{ }^\circ\text{K}^{-1}$ ,  $\rho = 1000 \text{ kg m}^{-3}$  and  $c_p/m_\nu = 4810 \text{ J kg}^{-1} \text{ }^\circ\text{K}^{-1}$ .

### C. Hydrocarbon Cryogen

Eqn. (1) dictates that  $T_1 - T_0$  be as large as as possible and  $\xi$  be as small as possible. For reasons explained more fully in Section III, the properties of solar salt determine  $T_1^+ = 823^\circ\text{K}$ ,  $T_1 = 495^\circ\text{K}$  and thus  $\xi = T_1^+/T_1 = 1.66$ . It remains to make  $T_0$  as low as possible. However, once  $T_0$  gets so low that  $T_0^+ < T_1$ , these two temperatures effectively switch roles.  $T_0^+$  must then be greater than  $T_{\text{dump}}$ , since there would otherwise be no way to re-initialize the engine after it had stopped and equilibrated with the environment. Thus  $T_0 = 300^\circ\text{K}/\xi = 180^\circ\text{K}$ .

For the purposes of this paper, second storage fluid will be prototyped as *n*-hexane. All fluids that remain liquid between  $180^\circ\text{K}$  and  $300^\circ\text{K}$  with vapor pressure less than 1 atmosphere are hydrocarbons or derivatives of them, so their physical properties are similar, and they all have

Ar	$p = 1.0 \times 10^6$ Pa					$p = 3.55 \times 10^6$ Pa				
	$T$ (°K)	$\mu$ (Pa sec)	$\kappa$ (W m <sup>-1</sup> °K <sup>-1</sup> )	$\rho RT/(m_\nu p)$	$\gamma$	Pr	$\mu$ (Pa sec)	$\kappa$ (W m <sup>-1</sup> °K <sup>-1</sup> )	$\rho RT/(m_\nu p)$	$\gamma$
180	$1.482 \times 10^{-5}$	$1.178 \times 10^{-2}$	1.041	1.769	0.715	$1.620 \times 10^{-5}$	$1.406 \times 10^{-2}$	1.180	2.167	0.872
240	$1.898 \times 10^{-5}$	$1.501 \times 10^{-2}$	1.014	1.716	0.685	$1.981 \times 10^{-5}$	$1.634 \times 10^{-2}$	1.055	1.857	0.731
300	$2.286 \times 10^{-5}$	$1.801 \times 10^{-2}$	1.005	1.695	0.676	$2.347 \times 10^{-5}$	$1.903 \times 10^{-2}$	1.019	1.771	0.696
398	$2.865 \times 10^{-5}$	$2.251 \times 10^{-2}$	0.999	1.681	0.670	$2.908 \times 10^{-5}$	$2.329 \times 10^{-2}$	0.999	1.718	0.676
495	$3.385 \times 10^{-5}$	$2.656 \times 10^{-2}$	0.997	1.675	0.668	$3.418 \times 10^{-5}$	$2.720 \times 10^{-2}$	0.992	1.697	0.670
659	$4.174 \times 10^{-5}$	$3.269 \times 10^{-2}$	0.996	1.671	0.667	$4.198 \times 10^{-5}$	$3.321 \times 10^{-2}$	0.990	1.681	0.666
823	$4.724 \times 10^{-5}$	$3.700 \times 10^{-2}$	0.996	1.667	0.666	$4.749 \times 10^{-5}$	$3.753 \times 10^{-2}$	0.989	1.673	0.665

N <sub>2</sub>	$p = 1.0 \times 10^6$ Pa					$p = 6.52 \times 10^6$ Pa				
	$T$ (°K)	$\mu$ (Pa sec)	$\kappa$ (W m <sup>-1</sup> °K <sup>-1</sup> )	$\rho RT/(m_\nu p)$	$\gamma$	Pr	$\mu$ (Pa sec)	$\kappa$ (W m <sup>-1</sup> °K <sup>-1</sup> )	$\rho RT/(m_\nu p)$	$\gamma$
180	$1.208 \times 10^{-5}$	$1.752 \times 10^{-2}$	1.033	1.462	0.759	$1.489 \times 10^{-5}$	$2.465 \times 10^{-2}$	1.238	2.010	0.990
240	$1.519 \times 10^{-5}$	$2.205 \times 10^{-2}$	1.010	1.429	0.735	$1.667 \times 10^{-5}$	$2.597 \times 10^{-2}$	1.051	1.607	0.794
300	$1.804 \times 10^{-5}$	$2.617 \times 10^{-2}$	1.002	1.417	0.728	$1.909 \times 10^{-5}$	$2.900 \times 10^{-2}$	1.002	1.509	0.753
398	$2.224 \times 10^{-5}$	$3.232 \times 10^{-2}$	0.998	1.406	0.724	$2.297 \times 10^{-5}$	$3.427 \times 10^{-2}$	0.979	1.450	0.734
495	$2.598 \times 10^{-5}$	$3.804 \times 10^{-2}$	0.996	1.396	0.724	$2.654 \times 10^{-5}$	$3.952 \times 10^{-2}$	0.973	1.422	0.729
659	$3.162 \times 10^{-5}$	$4.742 \times 10^{-2}$	0.996	1.377	0.727	$3.203 \times 10^{-5}$	$4.847 \times 10^{-2}$	0.973	1.389	0.730
823	$3.666 \times 10^{-5}$	$5.658 \times 10^{-2}$	0.997	1.358	0.732	$3.699 \times 10^{-5}$	$5.738 \times 10^{-2}$	0.975	1.365	0.733

TABLE II: Thermophysical properties of working fluids Ar and N<sub>2</sub>.<sup>53</sup> Both gases approach their liquid-vapor critical points at the lowest temperatures but are otherwise highly ideal. The specific heat ratios  $\gamma = c_p/c_v$  are well approximated by the equipartition values of 5/3 and 7/5. The molar masses  $m_\nu$  of 0.040 kg mole<sup>-1</sup> and 0.028 kg mole<sup>-1</sup> affect both the viscosity  $\mu$  and thermal conductivity  $\kappa$  but cancel out in the Prandtl number  $Pr = \mu c_p/(m_\nu \kappa)$ , which lies close to the ideal value of  $4\gamma/(9\gamma - 5)$  in both cases.

health and safety issues that must be weighed. Hexane, a component of gasoline, is pervasive, biodegradable, and cheap, and it is widely used in the food industry for extracting oils from seeds, but it is also highly flammable and neurotoxic.<sup>38-42</sup> Anhydrous methanol, to which hexane is physically similar, and which is an acceptable substitute, is vastly more toxic. All the lower alcohols—methanol, ethanol, propanol and propylene glycol—are hygroscopic and become viscous, like honey, at cryogenic temperatures when mixed with water.<sup>43,44</sup> Hydrocarbons can be rendered flame-resistant through halogenation, and a fluid such as CH<sub>2</sub>Cl<sub>2</sub> would work perfectly well, although it would increase the stress on stratospheric ozone.<sup>45,46</sup>

Fig. 5 shows the important thermophysical properties of *n*-hexane over the temperature range of interest.<sup>47-53</sup>

#### D. Working Fluid

The working fluid in this application is limited to gases that are extremely stable at high temperatures and far from liquefaction or solidification phase transitions at mildly cryogenic ones. The mechanical advantages of working near a critical point are outweighed in this case by unacceptability of fluid raining or snowing out and damaging the turbine blades. This eliminates, in par-

ticular, CO<sub>2</sub>, which has both liquefaction and freezing transitions in the range of 200°-300°K. These considerations plus requirements of chemical inertness and environmental friendliness restrict the possibilities to Ar and N<sub>2</sub>. The advantages of a lowered compression ratio and, potentially, higher adiabatic efficiency by using a gas with no internal degrees of freedom point to Ar as the preferred choice. However, N<sub>2</sub> has the advantage of requiring only minor modifications of rotor and stator airfoil shapes already optimized for use in air-breathing jet engines.<sup>54</sup>

Table II show the thermophysical properties of Ar and N<sub>2</sub> over the temperature and pressure range of interest.<sup>53</sup> Both gases are functionally ideal (and thus polytropic) except at the lowest temperatures. The correct low-temperature equation of state must be used in fine-tuning the turbomachinery, but the ideal equation of state is sufficient for making efficiency and cost estimates.

### III. REGENERATION

The practical materials limitations described in Section II require  $T_0^+ < T_1$ . As shown in Fig. 6, this condition causes heat transfers on the high-pressure and low-pressure sides of the circuit to overlap, thus eliminating the need to actually transfer heat to or from the stor-

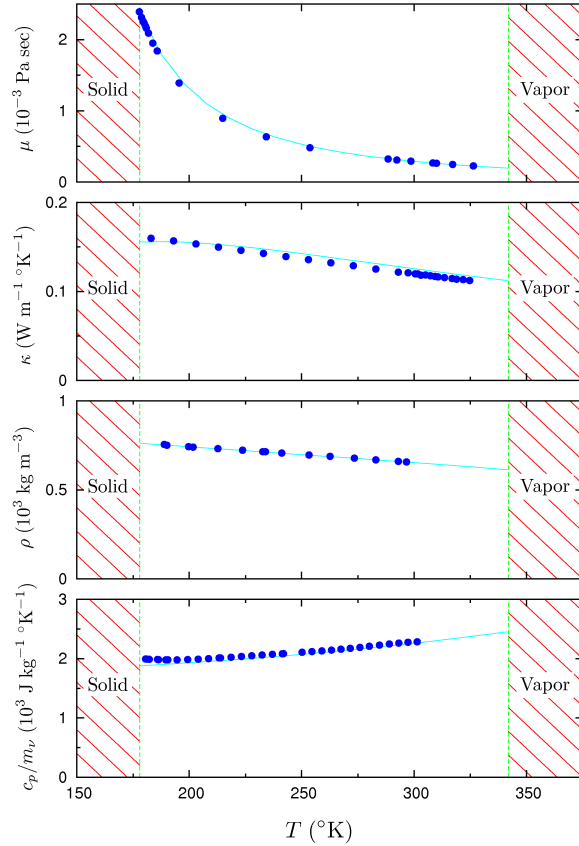


FIG. 5: Thermophysical properties of  $n$ -hexane ( $C_6H_{14}$ ). The melting and boiling temperatures at 1 atmosphere are  $179^\circ\text{K}$  and  $350^\circ\text{K}$ , respectively. The data are from various sources in the literature.<sup>47–52</sup> The lines are from the NIST standard reference database.<sup>53</sup> The temperature calibration of Giller and Drickamer has been adjusted 3% to agree with the accepted melting temperature.<sup>49</sup> The molar mass per formula unit is  $m_\nu = 0.086\text{ kg mol}^{-1}$ . The equipartition capacity with hydrogen motion frozen is  $c_p^{ideal}/m_\nu = 18R/m_\nu = 1740\text{ J }^\circ\text{K}^{-1}\text{ kg}^{-1}$ .

age fluids over this temperature range. Instead heat may simply be transferred directly from one side of the circuit to the other through a gas-gas heat exchanger, referred to as a regenerator, or recuperator.<sup>58</sup> In the limit that the entropy generation by the heat exchangers is zero, regeneration has no effect at all on the round-trip efficiency but simply reduces the amount of heat exchanger steel required. It also reduces the temperature ranges over which the storage fluids are required to be liquid. A modified version of Fig. 1 with regeneration included is shown in Fig. 7.

Figs. 6 and 7 clarify why  $T_0^+$  cannot exceed  $T_{dump}$ . An engine powered down and equilibrated to  $T_{dump}$  could easily be re-initialized by heating the (frozen) solar salt from  $T_{dump}$  to  $T_1$ , but it would not be easy to re-initialize if  $T_0^+$  had to be cooled to a value less than  $T_{dump}$ .

Fig. 6 justifies choosing  $T_1$  to be the solar salt melting

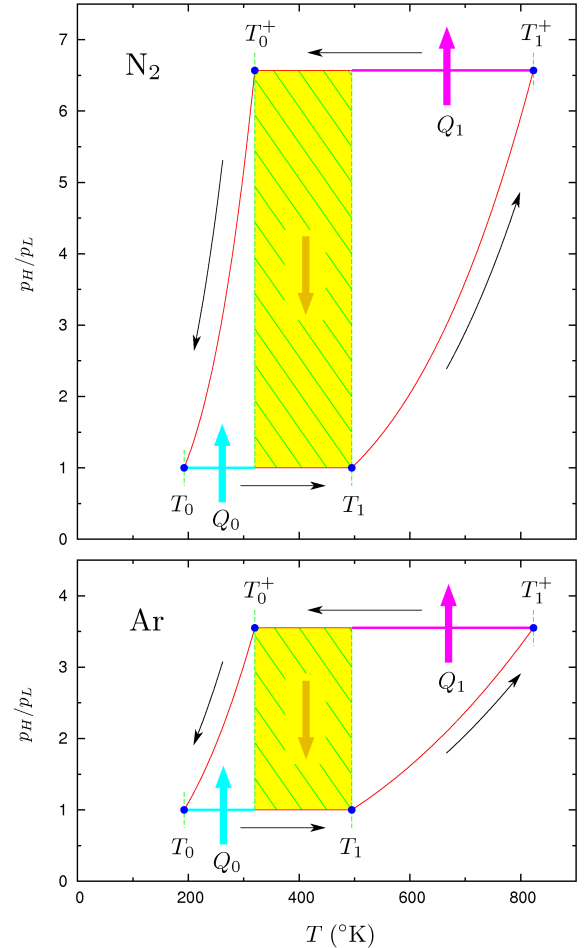


FIG. 6: Pressure-temperature diagrams for both Ar and  $N_2$  working fluids. The parameters are those in Table I. The system is shown in storage mode, following Fig. 1. Energy extraction is achieved by reversing all of the heat and fluid flows. In the temperature range  $T_0^+ < T < T_1$  (hatched region), heat is transferred directly between the high-pressure and low-pressure sides of the circuit by means of a gas-gas heat exchanger. The remaining heat exchanges with storage fluids when  $\nu$  moles of gas travel around the circuit are  $Q_0 = \nu c_p T_0 (\xi - 1)$  and  $Q_1 = \nu c_p T_1 (\xi - 1)$ .

point. With  $T_1^+$  and  $T_0^+$  fixed at the solar salt decomposition temperature and ambient, respectively, Eqn. (1) is maximized when  $\xi \ln(\xi)/(\xi - 1)$  is minimized. However, it may be seen from the plot of this function in Fig. 8 that the minimum occurs at  $\xi \rightarrow 1$ . Other costs not included in the calculation run away in this limit, so the specific value  $\xi = 1$  is not meaningful. However, the convergence of the function itself to 1 in this limit has the important implication that there is no significant round-trip efficiency penalty for  $1 < \xi < 2$ . Virtually any value of  $\xi$  in this range will do. Moreover, lowering  $T_1$  degrades the efficiency rather than improving it. There is thus no efficiency advantage in employing specialty salts with lower melting temperatures.

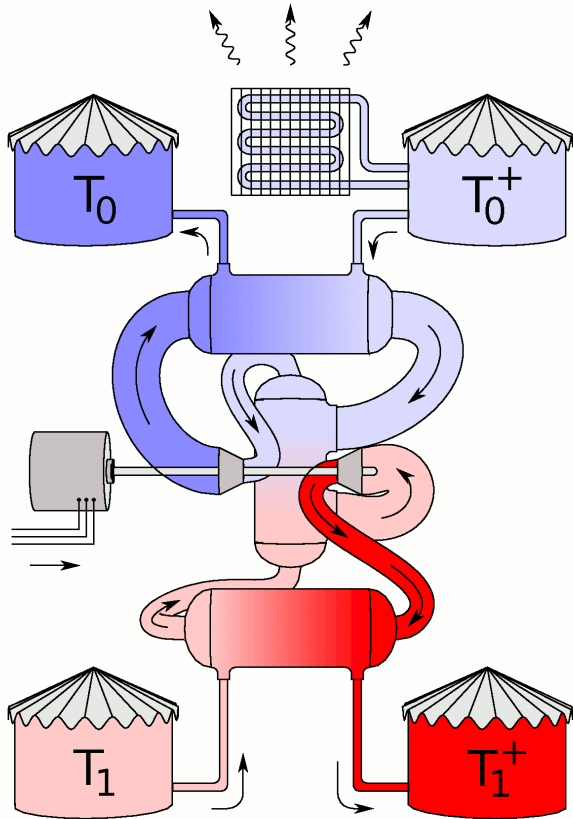


FIG. 7: Diagram of pumped thermal storage with heat exchange and regeneration. It is conceptually the same as Fig. 1 but has the roles  $T_1$  and  $T_0^+$  reversed. The heat flows are as shown in Fig. 6.

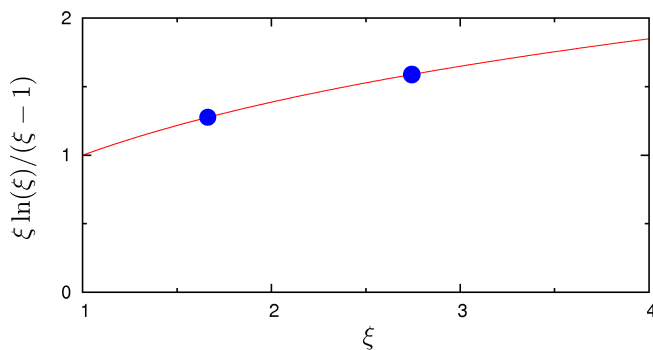


FIG. 8: Plot of the merit function  $\xi \ln(\xi)/(\xi - 1)$  implicit in Eqn. (1) with the values of  $T_0^+$  and  $T_1^+$  held fixed. The two circles correspond to  $\xi = 823^\circ\text{K}/495^\circ\text{K} = 1.66$  and  $\xi = 823^\circ\text{K}/300^\circ\text{K} = 2.74$ . This shows that  $\text{NaNO}_3/\text{KNO}_3$  eutectic is nearly optimal as a storage medium and that round-trip efficiency is actually degraded by substitution of specialty salts with lower melting points.

## IV. ROUND-TRIP EFFICIENCY

### A. Fictive Temperature

The round-trip storage efficiency  $\eta_{store}$  is most simply computed through the entropy budget. The system entropy  $S$  must be the same before and after a storage cycle because it is a property of state, so any entropy  $\Delta S$  generated during the cycle must be discarded as waste heat  $T_{dump}\Delta S$ , where  $T_{dump}$  is the slough temperature, roughly ambient. This heat represents a loss from the stored energy  $E_{store}$  that cannot be re-transmitted as grid power. We thus have

$$\eta_{store} < 1 - \frac{T_{dump}}{T_f} \quad \left( \frac{1}{T_f} = \frac{\Delta S}{E_{store}} \right) \quad (2)$$

The main contributions to the fictive temperature  $T_f$  come from the turbomachinery and three heat exchangers.

$$\frac{1}{T_f} = \frac{1}{T_f^{turbo}} + \sum \frac{1}{T_f^{hx}} \quad (3)$$

Other losses such as generator/motor inefficiency, unmanaged turbulence, and viscous drag in the conduits are percent-level corrections.

### B. Turbomachinery

In an adiabatic (entropy-conserving) compression or expansion, the temperature change  $dT$  resulting from a pressure change  $dp$  satisfies

$$\frac{dT}{T} = \left( \frac{\gamma - 1}{\gamma} \right) \frac{dp}{p} \quad (4)$$

where  $\gamma = c_p/c_v$ . In the limit that the turbomachinery is perfectly adiabatic, the temperature ratio  $\xi$  in Fig. 1 is thus related to the ratio of the upper and low pressures  $p_h/p_l$  by

$$\xi = T_0^+/T_0 = T_1^+/T_1 = \left( \frac{p_h}{p_l} \right)^{(\gamma-1)/\gamma} \quad (5)$$

In a real turbocompressor, Eqn (4) is modified to

$$\frac{dT}{T} = \frac{1}{\eta_c} \left( \frac{\gamma - 1}{\gamma} \right) \frac{dp}{p} \quad (6)$$

where  $\eta_c$  is the compressor polytropic efficiency. This slightly elevates the discharge temperature with respect to the ideal one for a given compression ratio. Integrating between the ideal temperature and the actual one at

constant pressure gives for the entropy created when  $\nu$  moles of gas pass through the compressor

$$\Delta S_c = \int \frac{\nu c_p}{T} dT = \nu c_p \left( \frac{1}{\eta_c} - 1 \right) \ln(\xi) \quad (7)$$

From the version of Eqn. (6) appropriate for the turbine

$$\frac{dT}{T} = \eta_t \left( \frac{\gamma - 1}{\gamma} \right) \frac{dp}{p} \quad (8)$$

one obtains similarly for the entropy created when  $\nu$  moles of gas expand through the turbine

$$\Delta S_t = \int \frac{\nu c_p}{T} dT = \nu c_p (1 - \eta_t) \ln(\xi) \quad (9)$$

Since the energy stored by cycling  $\nu$  mole of gas is  $E_{store} = (T_1 - T_0)(\xi - 1)\nu c_p$ , the inverse fictive temperature of the turbomachinery is

$$\frac{1}{T_f^{turbo}} = \frac{2(\Delta S_c + \Delta S_t)}{E_{store}} = \frac{2}{T_1 - T_0} \left( \frac{1}{\eta_c} - \eta_t \right) \frac{\ln(\xi)}{\xi - 1} \quad (10)$$

The factor of 2 accounts for summing the entropy generated during the storage and extraction steps. Eqn. (1) is obtained by substituting this expression into Eqn. (2).

The parameters of Table I give

$$T_f^{turbo} = 1210^\circ \text{K} \quad (11)$$

The values of  $\eta_c$  and  $\eta_t$  leading to this result lie at the extreme high end of present-day gas turbine technology.<sup>59-63</sup> They are benchmarked in the GE 90 aircraft engine. They are not characteristic of turbomachinery generally, however, so custom design is required to achieve them in practice. Turbomachinery bought off the shelf is a product fine-tuned to specific market needs that require a different set of compromises. There are theoretical indications that  $\eta_c$  and  $\eta_t$  could each be improved a further 1%.<sup>64-67</sup>

### C. Heat Exchangers

The fictive temperature of a heat exchanger differs from that of the turbomachinery in depending on both size and power. The physical principles are elementary and equally applicable to all heat exchanger designs, so the simple shell-and-tube prototype of Fig. 9 suffices for estimating the amount of steel required to achieve a given fictive temperature, even if more advanced designs are actually employed.<sup>70,71</sup>

The laminar and turbulent cases are both important. The Reynolds number inside a heat exchanger tube is

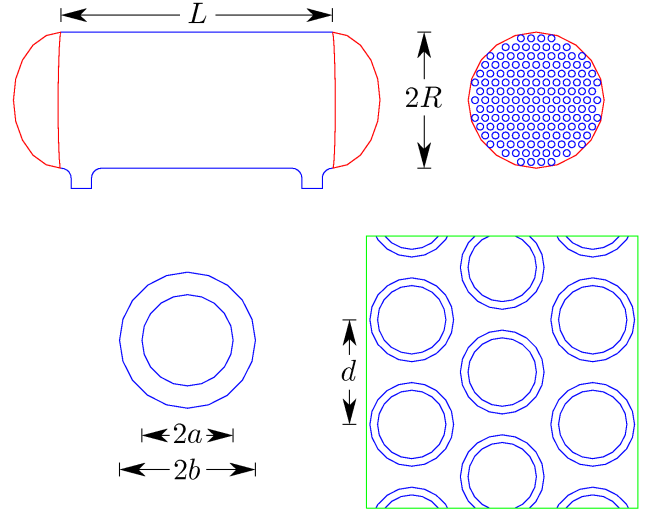


FIG. 9: Illustration of shell-and-tube prototype for heat exchanger. The number of tubes shown is  $N = 151$ . The lower right shows the case of  $b/a = 1.224$  and  $d/b = 1.25$ . The lower left shows the case of  $b/a = 1.491$ .

$$Re = \frac{2}{N\pi a} \left( \frac{m_\nu \dot{\nu}}{\mu} \right) \quad (12)$$

where  $a$  is the tube inner radius,  $N$  is the number of tubes, and  $\dot{\nu}$  is the number of moles of working fluid passing through the circuit per unit time. The flow is laminar if  $Re < 2000$ , turbulent if  $Re > 3000$  and intermittent otherwise. For this particular application, the effects of turbulence are adequately accounted for by replacing  $\mu$  and  $\kappa$  in the laminar expressions by the Darcy-Weisbach formula<sup>55,56</sup>

$$\tilde{\mu} = \mu \left[ \left( \frac{Re}{64} \right) f \right] \quad (13)$$

with the Swamee-Jain approximation for the Darcy friction factor

$$f = 0.25 \left[ \log_{10} \left( \frac{\epsilon}{7.4a} + \frac{5.74}{Re^{0.9}} \right) \right]^{-2} \quad (14)$$

and the Gnielinski correlation

$$\tilde{\kappa} = \kappa \left( \frac{11}{48} \right) \left[ \frac{(f/8)(Re - 1000)Pr}{1.0 + 12.7(f/8)^{1/2}(Pr^{2/3} - 1)} \right] \quad (15)$$

where  $Pr = \mu c_p / (m_\nu \kappa)$  is the Prandtl number. Fig. 10 shows these modifications to  $\mu$  and  $\kappa$  for various values of the tube surface roughness parameter  $\epsilon$ .

The laminar case follows from elementary considerations. Assuming a pressure gradient  $\partial p / \partial z$  along the tube and solving the Navier-Stokes equation

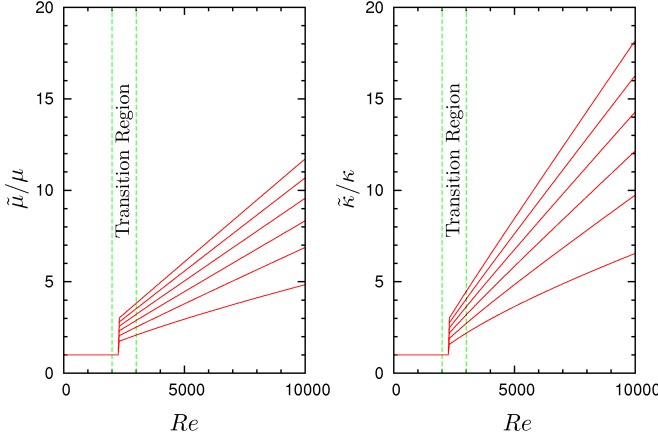


FIG. 10: Plot of turbulent enhancements of  $\mu$  and  $\kappa$  defined by Eqns. (13) and (15) for  $Pr = 2/3$  and surface roughness values  $\epsilon/(2a) = 0.00, 0.01, 0.02, 0.03, 0.04, 0.05$ .

$$\mu \left( \frac{\partial^2}{\partial r^2} + \frac{1}{r} \frac{\partial}{\partial r} \right) v_z = \frac{\partial p}{\partial z} \quad (16)$$

with a no-slip boundary condition, one obtains Hagen-Poiseuille flow

$$v_z = \frac{1}{4\mu} \left( \frac{\partial p}{\partial z} \right) (r^2 - a^2) \quad (17)$$

and an entropy generation due to viscous drag inside the tubes of

$$\dot{S}_{visc}^{(in)} = -\frac{2\pi N}{T} \int_0^a \left( \frac{\partial p}{\partial z} \right) v_z r dr = \left( \frac{8\mu}{\pi a^4} \right) \frac{TL}{N} \left( \frac{R\dot{V}}{p} \right)^2 \quad (18)$$

Assuming a temperature gradient  $\partial T/\partial z$  along the tube and similarly solving the heat flow equation

$$\kappa \left( \frac{\partial^2}{\partial r^2} + \frac{1}{r} \frac{\partial}{\partial r} \right) \delta T = c_p \left( \frac{p}{RT} \right) \left( \frac{\partial T}{\partial z} \right) v_z \quad (19)$$

one obtains the Graetz solution

$$\delta T = \frac{1}{\kappa} \left( \frac{\partial T}{\partial z} \right) \left( \frac{c_p \dot{V}}{N} \right) \frac{r^2 (r^2 - 4a^2 + 3a^4)}{8\pi a^4} \quad (20)$$

from which the entropy generation due to thermal resistance inside the tubes is computed to be

$$\begin{aligned} \dot{S}_{therm}^{(in)} &= -\frac{2\pi\kappa NL}{T^2} \int_0^a \left[ \frac{\partial(\delta T)}{\partial r} \right]^2 r dr \\ &= \frac{11}{48\pi\kappa} \left( \frac{L}{N} \right) \left[ \left( \frac{\partial T}{\partial z} \right) \frac{c_p \dot{V}}{T} \right]^2 \end{aligned} \quad (21)$$

These two contributions to  $\dot{S}^{(in)}$  become equal when the heat exchanger length is  $L_0$ , defined by

$$\sqrt{\frac{384}{11}} \frac{\ell L_0}{a^2} = \left( \frac{\gamma}{\gamma - 1} \right) \frac{\Delta T}{T} \quad (22)$$

where  $\Delta T$  is the temperature difference between the two ends of the heat exchanger and

$$\ell = \frac{\sqrt{\kappa\mu T}}{p} \quad (23)$$

is the working fluid scattering mean free path.<sup>57</sup> The entropy creation outside the tube is a multiple of  $\dot{S}^{(in)}$  obtained by solving Eqns. (16) and (19) numerically for a given value of  $d$ . The result is summarized in Table III. The fictive temperature is then

$$\begin{aligned} \frac{1}{T_f^{hx}} &= \frac{11}{24\pi\kappa} \left[ \frac{\Delta T}{T} \frac{1}{(T_1 - T_0)(\xi - 1)} \right]^2 \\ &\times \left[ 1 + \frac{\dot{S}^{(out)}}{\dot{S}^{(in)}} \right] \left( 1 + \frac{L^2}{L_0^2} \right) \frac{\dot{E}}{NL} \end{aligned} \quad (24)$$

where  $\dot{E}$  is the engine power. The factor of 2 accounts for entropy creation during both the storage and extraction steps. Entropy creation due to heat flow in the steel is irrelevant in this application.

There is no need to make the heat exchanger fictive temperature more than about 30 times  $T_f^{turbo}$ . A set of parameters that gives  $T_f^{hx}$  in this range for laminar flow is shown Table III. The important quantity for costing purposes is the steel mass per engine watt

$$\frac{M}{\dot{E}} = \rho_{steel} \pi (b^2 - a^2) L \left( \frac{N}{\dot{E}} \right) \quad (25)$$

Here  $N/\dot{E}$  is the number of tubes per engine watt, given by

$$\frac{N}{\dot{E}} = \frac{2}{\pi a Re} \left( \frac{m_\nu}{c_p \mu} \right) \frac{1}{(T_1 - T_0)(\xi - 1)} \quad (26)$$

per Eqn. (12). Both  $M/\dot{E}$  and  $T_f^{hx}$  remain unchanged if  $L$  is made smaller keeping  $NL$  fixed (which requires lowering  $Re$ ). Thus Table III actually describes a family of designs with different aspect ratios but similar performance characteristics.

Making  $L$  longer keeping  $NL$  fixed pushes  $Re$  over the turbulence threshold. As shown in Table IV, this causes a 50% reduction in  $M/\dot{E}$  for the same value of  $T_f$ . This occurs because the turbulent enhancement of the thermal conductivity matters more than turbulent enhancement of the viscosity when  $L < L_0$ . Thus the optimal design

Ar	Low	Regen	High
$T$	240°K	398°K	659°K
$\Delta T$	120°K	195°K	327°K
$p^{(in)}$	$1.00 \times 10^6$ Pa	$3.55 \times 10^6$ Pa	$3.55 \times 10^6$ Pa
$p^{(out)}$	$1.00 \times 10^5$ Pa	$1.00 \times 10^6$ Pa	$1.00 \times 10^5$ Pa
$\sigma_{max}$	$1.30 \times 10^8$ Pa	$1.30 \times 10^8$ Pa	$1.00 \times 10^8$ Pa
$b/a$	1.224	1.224	1.491
$d/b$	2.500	4.259	2.500
$\dot{S}^{(out)}/\dot{S}^{(in)}$	0.0182	0.6429	0.0119
$\ell$	$8.27 \times 10^{-9}$ m	$4.62 \times 10^{-9}$ m	$8.54 \times 10^{-9}$ m
$a$	0.0015 m	0.0015 m	0.0015 m
$L_0$	55.2 m	96.5 m	54.6 m
$L$	20.0 m	30.0 m	20.0 m
$Re$	2000	2000	2000
$N/\dot{E}$	$0.0997 \text{ W}^{-1}$	$0.0651 \text{ W}^{-1}$	$0.0463 \text{ W}^{-1}$
$M/\dot{E}$	$0.0551 \text{ kg W}^{-1}$	$0.0540 \text{ kg W}^{-1}$	$0.0629 \text{ kg W}^{-1}$
$T_f^{hx}$	30520°K	30880°K	31990°K

N <sub>2</sub>	Low	Regen	High
$T$	240°K	398°K	659°K
$\Delta T$	120°K	195°K	327°K
$p^{(in)}$	$1.00 \times 10^6$ Pa	$6.52 \times 10^6$ Pa	$6.52 \times 10^6$ Pa
$p^{(out)}$	$1.00 \times 10^5$ Pa	$1.00 \times 10^6$ Pa	$1.00 \times 10^5$ Pa
$\sigma_{max}$	$1.30 \times 10^8$ Pa	$1.30 \times 10^8$ Pa	$1.00 \times 10^8$ Pa
$b/a$	1.224	1.224	1.491
$d/b$	2.500	5.047	2.500
$\dot{S}^{(out)}/\dot{S}^{(in)}$	0.0268	0.7943	0.0209
$\ell$	$8.97 \times 10^{-9}$ m	$2.72 \times 10^{-9}$ m	$4.91 \times 10^{-9}$ m
$a$	0.0015 m	0.0015 m	0.0015 m
$L_0$	70.7 m	221.4 m	137.5 m
$L$	20.0 m	30.0 m	20.0 m
$Re$	2000	2000	2000
$N/\dot{E}$	$0.0632 \text{ W}^{-1}$	$0.0407 \text{ W}^{-1}$	$0.0290 \text{ W}^{-1}$
$M/\dot{E}$	$0.0350 \text{ kg W}^{-1}$	$0.0338 \text{ kg W}^{-1}$	$0.0393 \text{ kg w}^{-1}$
$T_f^{hx}$	29540°K	28050°K	32150°K

TABLE III: Prototypical heat exchanger parameters for laminar case. The inner radius  $a$  is set to the smallest size heat exchanger tubing available commercially from multiple sources. The base value of  $b/a$  is the sum of the pure stress component from Eqn. (27), which is relatively small, and a milling tolerance factor of 11.2% taken the Los Alamos Engineering Standards Manual PD342 for this size tube. This brings the tubes into compliance with ASME B31.3 which is more strict than is required for heat exchanger applications.<sup>68</sup> (ASTM guidelines require manufacturers to control tube wall width to at least 12.5% of the diameter.<sup>69</sup>) To this is added an extra  $4.0 \times 10^{-4}$  m for the salt heat exchanger as a corrosion margin. The value of  $d/b$  is fixed at the industry value of 2.5 except for the regenerator, where it is picked to minimize  $\dot{S}^{(out)}/\dot{S}^{(in)}$ . The Reynolds number  $Re$  is set to just below the turbulence threshold. The value of  $L$  is then adjusted to make  $T_f^{hx} \simeq 30000$ . The extra significant figures in this table are included to aid in checking calculations and are not predictive.

Ar	Low	Regen	High
$T$	240°K	398°K	659°K
$\Delta T$	120°K	195°K	327°K
$p^{(in)}$	$1.00 \times 10^6$ Pa	$3.55 \times 10^6$ Pa	$3.55 \times 10^6$ Pa
$p^{(out)}$	$1.00 \times 10^5$ Pa	$1.00 \times 10^6$ Pa	$1.00 \times 10^5$ Pa
$\sigma_{max}$	$1.30 \times 10^8$ Pa	$1.30 \times 10^8$ Pa	$1.00 \times 10^8$ Pa
$b/a$	1.224	1.224	1.491
$d/b$	2.500	4.258	2.500
$\dot{S}^{(out)}/\dot{S}^{(in)}$	0.0404	0.6429	0.0253
$\tilde{\ell}$	$1.78 \times 10^{-8}$ m	$9.91 \times 10^{-9}$ m	$1.82 \times 10^{-8}$ m
$a$	0.0015 m	0.0015 m	0.0015 m
$\tilde{L}_0$	25.7 m	45.0 m	25.6 m
$L$	20.0 m	30.0 m	20.0 m
$Re$	3000	3000	3000
$N/\dot{E}$	$0.0665 \text{ W}^{-1}$	$0.0434 \text{ W}^{-1}$	$0.0309 \text{ W}^{-1}$
$M/\dot{E}$	$0.0367 \text{ kg W}^{-1}$	$0.0360 \text{ kg W}^{-1}$	$0.0419 \text{ kg W}^{-1}$
$T_f^{hx}$	31040°K	34440°K	32420°K

N <sub>2</sub>	Low	Regen	High
$T$	240°K	398°K	659°K
$\Delta T$	120°K	195°K	327°K
$p^{(in)}$	$1.00 \times 10^6$ Pa	$6.52 \times 10^6$ Pa	$6.52 \times 10^6$ Pa
$p^{(out)}$	$1.00 \times 10^5$ Pa	$1.00 \times 10^6$ Pa	$1.00 \times 10^5$ Pa
$\sigma_{max}$	$1.30 \times 10^8$ Pa	$1.30 \times 10^8$ Pa	$1.00 \times 10^8$ Pa
$b/a$	1.224	1.224	1.491
$d/b$	2.500	5.047	2.500
$\dot{S}^{(out)}/\dot{S}^{(in)}$	0.0610	0.7942	0.0399
$\tilde{\ell}$	$1.95 \times 10^{-8}$ m	$5.91 \times 10^{-9}$ m	$1.07 \times 10^{-8}$ m
$a$	0.0015 m	0.0015 m	0.0015 m
$\tilde{L}_0$	32.5 m	101.7 m	63.3 m
$L$	20.0 m	30.0 m	20.0 m
$Re$	3000	3000	3000
$N/\dot{E}$	$0.0421 \text{ W}^{-1}$	$0.0272 \text{ W}^{-1}$	$0.0193 \text{ W}^{-1}$
$M/\dot{E}$	$0.0233 \text{ kg W}^{-1}$	$0.0225 \text{ kg W}^{-1}$	$0.0262 \text{ kg w}^{-1}$
$T_f^{hx}$	33920°K	39800°K	44280°K

TABLE IV: Same as Table III except with the Reynolds number  $Re$  raised above the turbulence threshold in the smooth-tube limit ( $\epsilon \rightarrow 0$ ). The quantities  $\tilde{\ell}$  and  $\tilde{L}_0$  are the same as  $\ell$  and  $L_0$  except computed with the turbulence-enhanced values of  $\tilde{\mu}$  and  $\tilde{\kappa}$  defined by Eqns. (13) and (15).  $T_f^{hx}$  is also computed using  $\tilde{\kappa}$ .

with respect to steel mass has  $Re$  just above the turbulence threshold. Further cost compromise at this value of  $Re$  may be made shortening  $L$  keeping  $N$  fixed, reducing both  $T_f$  and  $M/\dot{E}$  proportionately.

The choice of tube inner and outer radii  $a$  and  $b$  has no effect on  $T_f$  if  $Re$  and  $L$  are held fixed (and if  $L < L_0$ ), but it has a large effect on  $M/\dot{E}$ . Accordingly, the total cost of steel is minimized by making  $a$  as small as possible. The minimum value of  $b/a$  required for creep resistance is determined by

	Ar	N <sub>2</sub>
$T_f$	1089°K	1107°K
$\sum M/\dot{E}$	0.1136 kg W <sup>-1</sup>	0.0720 kg W <sup>-1</sup>
$T_{GT}^{ex}$	873°K	823°K
$\eta_{GT}$	0.38	0.038
$\partial\mathcal{C}_{GT}/\partial\dot{E}$	\$0.25 W <sup>-1</sup>	\$0.25 W <sup>-1</sup>
$\partial\mathcal{C}_{steel}/\partial M$	\$1.00 kg <sup>-1</sup>	\$1.00 kg <sup>-1</sup>
$\partial\mathcal{C}/\partial\dot{E}$	\$0.27 W <sup>-1</sup>	\$0.20 W <sup>-1</sup>
$\partial\mathcal{C}_{salt}/\partial M$	\$0.61 kg <sup>-1</sup>	\$0.61 kg <sup>-1</sup>
$\partial\mathcal{C}_{hex}/\partial M$	\$0.70 kg <sup>-1</sup>	\$0.70 kg <sup>-1</sup>
$\partial\mathcal{C}/\partial E$	$\$3.54 \times 10^{-6}$ J <sup>-1</sup>	$\$3.54 \times 10^{-6}$ J <sup>-1</sup>

TABLE V: Top: Parameters used in Eqn. (28) to estimate the cost per engine watt  $\partial\mathcal{C}/\partial\dot{E}$ . The total fictive temperature  $T_f$  is computed with Eqn. (3) using values in Table IV. The total mass per engine watt  $\sum M/\dot{E}$  is obtained by summing the values in Table IV. The standard gas turbine exhaust temperature  $T_{GT}^{ex}$  and thermodynamic efficiency  $\eta_{GT}$  are from Brooks.<sup>72</sup> The gas turbine cost per engine watt  $\partial\mathcal{C}_{GT}/\dot{E}$  is from Black and Veach, as reported by NREL.<sup>73</sup> The Black and Veach cost of 0.60 W<sup>-1</sup> for a simple cycle power plant upon which this estimate is based also agrees with Tidball *et al.*<sup>74</sup> The cited steel tubing price per kilogram  $\partial\mathcal{C}/\partial M$  is on the extreme low edge of the market range. Fenton quotes \$0.6 kg<sup>-1</sup> as the carbon steel price.<sup>75</sup> The price of stainless steel is typically 5 times the price of carbon steel. Bottom: Parameters used in Eqn (29) to estimate the marginal cost per stored joule  $\partial\mathcal{C}/\partial E$ . The nitrate eutectic cost per kilogram  $\partial\mathcal{C}_{salt}/\partial M$  is from Apodaca.<sup>76</sup> The hexane cost per kilogram  $\partial\mathcal{C}_{hex}/\partial M$  is taken to be the price of gasoline reported by the U.S. EIA.<sup>77</sup>

$$\frac{b^2 - a^2}{b^2 + a^2} \geq \frac{\Delta p}{\sigma_{max}} \quad (27)$$

where  $\Delta p$  is the pressure difference between the inside and outside of the tube and  $\sigma_{max}$  is the maximum stress allowed in the tube steel, shown in Fig. 2. To this minimal  $b/a$  must be added a mill tolerance margin, the default for which is a factor 1.25 (12.5% of diameter), and a salt corrosion margin, which is  $4.0 \times 10^{-4}$  m for a 40-year lifespan.<sup>68,69</sup> Thus it is impractical to make  $a$  much smaller than  $1.5 \times 10^{-3}$  in the high-temperature heat exchanger. The regenerator and low-temperature heat exchanger may involve microchannel designs of  $a = 5.0 \times 10^{-4}$  m, thus potentially lowering  $M/\dot{E}$  in those cases.<sup>70,71</sup>

## V. COST

The cost  $\mathcal{C}$  of grid storage has two distinct metrics: the cost per engine watt  $\partial\mathcal{C}/\partial\dot{E}$  and the cost per stored joule  $\partial\mathcal{C}/\partial E$ . The first is characteristic of the engine and depends only on how fast energy is transferred to and from

the grid, not on how much energy is stored or for how long. The second characterizes the storage medium and is completely independent of how fast energy is transferred in or out. One imagines first building the engine at a certain power rating (and cost) and then adding as much storage capacity as circumstances warrant.

A crude estimate of the cost per engine watt is

$$\frac{\partial\mathcal{C}}{\partial\dot{E}} = \frac{T_{GT}^{ex} - T_{dump}}{(T_1 - T_0)(\xi - 1)} \frac{\eta_{GT}}{1 - \eta_{GT}} \left(\frac{c_p^{N_2}}{c_p}\right) \left(\frac{p_0}{p_l}\right) \times \frac{\partial\mathcal{C}_{GT}}{\partial\dot{E}} + 2 \frac{\partial\mathcal{C}_{steel}}{\partial M} \sum \frac{M}{\dot{E}} \quad (28)$$

The definitions of these parameters and their values are summarized in Tables I and V.<sup>72-77</sup> This expression assumes that the cost of the turbomachinery is proportional to the number of moles per second  $\dot{\nu}$  passing through it, scaled to the ambient pressure. The marginal cost of the (very large) heat exchangers required is estimated at 2 times the cost of the steel used to make them. This estimate is consistent with the \$2 kg<sup>-1</sup> implicit in the heat-exchanger price figures of Loh *et al.*, assuming a tube width of 0.125 times the tube diameter, the standard ASME milling margin.<sup>78</sup>

A crude estimate for the marginal cost per stored joule is

$$\frac{\partial\mathcal{C}}{\partial E} = \frac{1}{(T_1 - T_0)(\xi - 1)} \times \left[ \left(\frac{m_{\nu}^{salt}}{c_p^{salt}}\right) \frac{\partial\mathcal{C}_{salt}}{\partial M} + \left(\frac{m_{\nu}^{hex}}{c_p^{hex}}\right) \frac{\partial\mathcal{C}_{hex}}{\partial M} \right] \quad (29)$$

The definitions of these parameters and their values are summarized in Tables I and V. Specifically omitted from this estimate because they are too small to matter are the costs of large storage tanks (\$50 m<sup>-3</sup>) and excavation (\$2.4 m<sup>-3</sup>).<sup>78-80</sup>

Eqns. (28) and (29) are oversimplified, and they leave out many obvious costs—flow handling, cooling structures, tanks, insulation, pumps, site preparation, small loss accounting. However, they are sufficiently accurate to reveal the broad-brush picture: The cost of the turbomachinery is lowered by the elevated pressure in the closed brayton loop so much that the cost per engine watt becomes dominated by the cost of the heat exchangers. The latter are conceptually trivial and scale up easily to arbitrarily large sizes. They become arbitrarily efficient when they do. Heat exchangers large enough to contribute negligibly to the total entropy budget can be built for a total cost per engine watt comparable to that of a present-day simple-cycle gas turbine. The marginal cost per stored joule, dominated by the cost of the storage fluids, is about  $\$3.54 \times 10^{-6}$  J<sup>-1</sup> (\$12.7 per kWh).

The plant cost curves associated with Table V are shown in Fig. 11. With the understanding that these

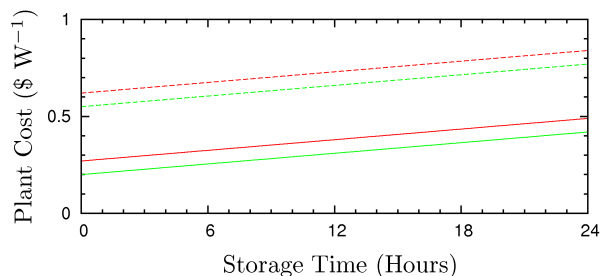


FIG. 11: Cost structure implicit in Table V. This should be understood as an illustration only because the error bars of Table V are very large. The base costs per engine watt  $\partial\mathcal{C}/\partial\dot{E}$  for Ar and  $\text{N}_2$  correspond to the two solid line intercepts at zero hours of storage time. The upper line is Ar. The slopes of these lines correspond to the marginal cost per stored joule  $\partial\mathcal{C}/\partial E$ . The dashed lines represent these quantities with  $\$0.35 \text{ W}^{-1}$  of infrastructure cost added (baffles, tanks, switchyard, buildings, etc.), the value needed to convert a  $\$0.24 \text{ W}^{-1}$  gas turbine into a full  $\$0.6 \text{ W}^{-1}$  simple-cycle power plant.<sup>73,74</sup>

are illustrations only, on account of the large error bars, one can see that the cost of the storage is negligible for storage times less than a day, and thus that only the costs per engine watt and plant infrastructure matter. There is, in particular, no significant economic advantage to substituting rocks for solar salt and hexane.

## VI. DISCUSSION

### A. Physical Constraints

Which storage technology actually prevails in the end will depend ultimately on cost, and this is something difficult to assess correctly without actually building machines and testing them. Thus it is not possible to make a purely economic case that the technology described here, which exists only as a concept, will win out. Rather the argument rests partly on such cost analysis as one can do combined with a little common sense.

It is highly reasonable, for example, from a physics perspective that the mechanical parts of thermal storage with heat exchange should cost less than pumped hydroelectric storage, the technology with which is it most closely related. The turbines are smaller by virtue of turning faster and having greater blade and fluid velocities. They require no burners or blade cooling. Salt and hexane store energy more compactly than water does when pumped uphill: One kg of water lifted 380 m, a typical pumped storage elevation drop, stores 0.7% of the energy that one kg of nitrate salt does when heated from  $T_1$  to  $T_1^+$ . One kg of water falling 380 m transmits 3.4% of the energy to the turbine blades that 1 kg of Ar working fluid does when it travels around the brayton circuit. In the case of  $\text{N}_2$  working fluid, it is 1.7%. Thermal storage

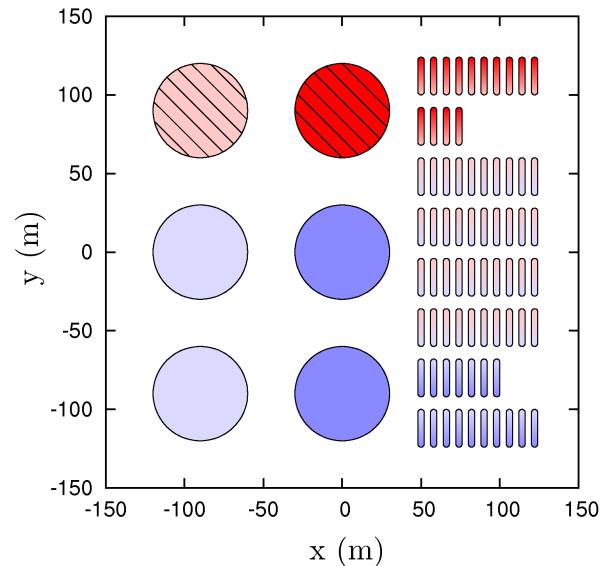


FIG. 12: Illustration of a thermal storage facility footprint showing the size scales involved. The parameters are those of Tables IV and V. The power is  $2.5 \times 10^8 \text{ W}$ . The storage time is 24 hours. The working fluid is Ar. The circles are oil depot storage tanks 14.0 meters tall and 30.0 m in radius.<sup>79</sup> The two hatched ones are for the nitrate salt (one each for two salt tanks in Figs. 1 and 7). The remaining four blue ones are for the hexane. The heat exchanger units are cylinders 20 m long and 2 m in radius, ganged in parallel. The turbomachinery is too compact to be drawn meaningfully on this diagram, but the turbine, compressor and generator together are about the size of one heat exchanger unit. The energy stored per unit are of footprint is  $2.5 \times 10^8 \text{ J m}^{-2}$ , or about 2-10 times the typical pumped hydroelectric storage value, reckoned from the upper reservoir area.<sup>81</sup> For reasons of minimizing mechanical load cycling on the tanks, a realistic design would probably store the hot and cold salt in the same tank with a thermal barrier between them, and similarly with the hexane, thus halving the number of tanks. The entire facility would also likely be underground, for thermal insulation reasons in the case of the tanks and for safety reasons in the case of the heat exchangers.

also uses less land than pumped hydroelectricity does—and, of course, requires no mountains or water supplies. This is shown explicitly Fig. 12, where the footprint of a prototypical storage facility based on oil depot storage tanks is sketched out.<sup>79</sup> Depending on construction details, the thermal storage land requirement can be 10% or less of the equivalent pumped hydroelectric storage requirement, reckoned from the upper reservoir area.<sup>81</sup>

It is also reasonable that the heat exchangers should cost only slightly more than the steel used to make them. This is so even though large heat exchangers with the specifications in Table IV do not presently exist as products at any price. Heat exchangers are the mechanical engineering equivalents of semiconductor memory chips or flat-panel displays: One makes them by repeating the same simple step over and over again millions of times.

That means their manufacture can be automated. Their manufacture has not yet been automated, but this is only because there is no market for such products. It would be quite straightforward to program industrial robots to perform this task at extremely low cost. A facility the size of Fig. 12 would require about  $3.0 \times 10^7$  tubes of length 20 m, or a total length of  $6.0 \times 10^8$  m, enough to circle the earth 15 times. The cost of building it would be prohibitive if humans were doing the work, but robots would be doing it.

### B. Heat versus Electrochemistry

Were batteries ever to beat the marginal cost per stored joule of pumped hydroelectric storage, the comparison with the latter would become moot. However, they have not done so yet, as the continued construction of new pumped storage facilities around the world demonstrates.<sup>82–85</sup> Why the battery cost problem remains so intractable is revealed by stored energy per unit mass, which varies between  $1.4 \times 10^5$  J kg<sup>-1</sup> for cheap lead-acid car batteries to  $9.5 \times 10^5$  J kg<sup>-1</sup> for high-end Li-ion batteries.<sup>86–88</sup> This is not significantly different from the  $c_p/m_\nu(T_1 - T_0)(\xi - 1) = 3.22 \times 10^5$  J kg<sup>-1</sup> of nitrate salt, notwithstanding the fact that an active atom in a battery stores 10 times more energy than atom of nitrate salt does. The extra mass is infrastructure, atoms that don't actually store any energy but guide electrons to the atoms that do. This extra mass is expensive, and one cannot significantly reduce it without making the battery more likely to short and explode. There are also lifetime issues associated with a battery's electrode degradation, particularly if it is deeply cycled, that translate into additional long-term maintenance cost.<sup>89</sup> This problem is fundamental because the electrode surface, the place where electron motion converts to ion motion, is a scene of violence on the atomic scale. Flow batteries and liquid metal batteries greatly reduce the electrode degradation problem, but they do so by means of engineering compromises that raise other costs.<sup>90–93</sup> It is not clear that either will be cheaper than mass-produced Li-ion batteries.<sup>94</sup>

Batteries also have environmental issues associated with their metal ions that have led to mandatory recycling and the banning of household battery disposal in landfills.<sup>95–99</sup> This issue does not exist with pumped thermal storage with heat exchange. If the facility of Fig. 12 had a catastrophic tank breach (and no fire) the stored energy would dissipate harmlessly as heat, and the result would be a patch of cold nitrate fertilizer that could be easily cleaned up and re-used. If, on the other hand, a vanadium flow battery of the same capacity (two such tanks are required) had such a breach,  $8.0 \times 10^6$  kg of vanadium ions would be dumped on the ground along with a comparable mass of sulfuric acid.

Thus, while batteries have an advantage over all other forms of storage at small scales in having no significant entry cost per engine watt, this advantage disappears

once the scale becomes large enough that the cost entry barrier is surmounted.

### C. Explosion Danger

With the exception of hydrogen electrolysis, which has cost and electrode issues similar to those of batteries, all other methods for storing grid-scale energy have nuclear-scale explosion dangers.<sup>100</sup> This includes in particular flywheels, high pressure tanks, and all purely electrical media such as supercapacitors and superconducting magnetic coils.<sup>101,102</sup> These media also have lower energy storage densities, but that is a secondary matter. In the case of flywheels and pressure vessels made out of steel, the maximum energy stored per unit mass of steel is  $\sigma_{max}/\rho_{steel}$ , or about 2.5% of the energy stored thermally per unit mass of nitrate salt. For supercapacitors, this factor is about 10%.

Deliberately excluded from the list of explosive technologies is compressed air storage in underground caverns.<sup>103,104</sup> This is a special case both because it is underground, and thus not explosive, and because it is functionally the same thing as thermal storage with heat exchange. The energy expended in compressing any gas is actually stored in its heat. Thus, adiabatically compressing N<sub>2</sub> from  $1.0 \times 10^5$  Pa to  $7.0 \times 10^6$  Pa (70 atmospheres), the typical underground storage pressure, raises its temperature from 300°K to 1101°K. Placing such hot gas underground just to cool off there would make no sense, so all compressed air storage technologies with high round-trip efficiencies employ above-ground heat exchangers like those of Figs. 1 and 7 to cool the gas (extract energy from it) before pumping it underground.<sup>105–109</sup> Heat is then added back to the gas as it expands in the extraction step. Thus the only difference between underground storage and pure thermal storage with heat exchange is that the latter sends the working fluid through the brayton cycle twice so as to eliminate the need to store working fluid at pressure at all—and thus to eliminate the need for the cavern.

Pumped thermal storage with heat exchange does have explosion danger. It is associated with the heat exchangers, however, not the storage media, so it scales with engine power rather than total stored energy. The parameters in Table IV give a total explosive energy of 90 seconds worth of generation at the design power, whatever it is, for Ar and 166 seconds for N<sub>2</sub>. Thus, for the configuration of Fig. 12, the explosive power for Ar is  $2.25 \times 10^{10}$  joules, or 4.8 tons of TNT. Heat exchange units of this size and pressure are common in the petrochemical industry, and it is known that they explode rarely, but that when they do the result is catastrophic.<sup>110</sup> Thus precautions must be taken to make sure that any tank explosion that might occur does not cascade, for example by siting the units underground.

Another serious difficulty is the cost associated with managing the working fluid inventory in case of breach.

Both Ar and N<sub>2</sub> are asphyxiating gases. They are quite deadly until they dissipate in the atmosphere. The total working fluid inventory in the case of Fig. 12 is  $2.7 \times 10^5$  kg of Ar. For comparison, the total amount of CO<sub>2</sub> released in the Lake Nyos disaster is estimated to be  $10^9$  kg.<sup>111</sup>

#### D. Additional Technical Issues

The power of pumped thermal storage with heat exchange is governed by adjusting the working fluid inventory up and down. The large heat capacity of the heat exchanger steel and corresponding slow thermal response call for regulating the storage fluid flow so as to keep the temperatures fixed. The power the working fluid delivers to the grid or absorbs from it is then directly proportional to the number of moles passing a given point per second. Since a motor/generator connected to the grid is phase-locked with other generators through electric forces, the working fluid flow velocity is essentially fixed, and this means that one governs the power by reducing or increasing the background pressure of the working fluid in the circuit.

Two sets of turbomachinery may be required, one for storage and another for extraction. For the parameters in Tables IV and V, this would raise the cost per engine watt by about  $\$0.05 \text{ W}^{-1}$ . In contrast to the situation in pumped hydroelectricity, the turbomachinery in this case cannot be automatically reversed because the blades are air foils carefully crafted for maximum efficiency under specific operating conditions, notably flow direction and mach number. It is possible to design reversible air foils, but it is not presently known how much efficiency compromise would be required to make machinery that worked equally well in both directions. The worst-case scenario is that no set of air foils would perform this task adequately, in which case two sets of turbomachinery would be required. The cost of doubling the turbomachinery becomes less and less of an issue as the pressure is raised.

The brayton cycle requires closing. This is most conveniently accomplished using slightly different compression ratios for storage and generation, as shown in Fig. 13. Choosing these to make  $T_1^+$  match causes the heat to be dumped at the lowest possible temperature. In place of Eqn. (1) we then have

$$\eta_{store} < 1 - \frac{T_0}{T_1 - T_0} \left[ \frac{\xi^{1/\eta_c \eta_t} - \xi^{\eta_c \eta_t}}{\xi - 1} \right] \quad (30)$$

The parameters in Table I give  $\eta_{store} < 0.75$ , in agreement with Eqn. (1). This number is too high, however, because  $T_0^{+(store)}$  cannot lie below ambient. Taking ambient to be  $300^\circ\text{K}$ , we obtain  $T_0 = 195^\circ\text{K}$  and thus  $\eta_{store} < 0.72$ .

In contrast to pumped hydroelectric and electrochemical storage, pumped thermal storage does not actually

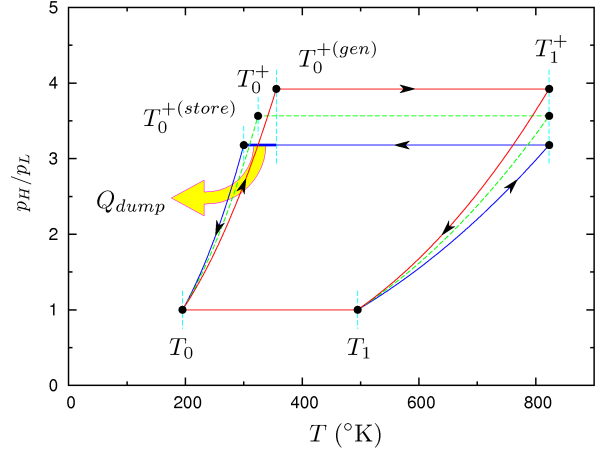


FIG. 13: Illustration of a fully closed brayton cycle for the case of Ar working fluid. The storage and extraction cycles have their compression ratios modified to  $\xi^{\eta_c \gamma / (\gamma - 1)}$  and  $\xi^{\gamma / (\gamma - 1) \eta_t}$ , respectively, so as to cause  $T_1^+$  to match. This causes a mismatch between  $T_0^{+(store)} = T_0 \xi^{\eta_c \eta_t}$  and  $T_0^{+(gen)} = T_0 \xi^{1/\eta_c \eta_t}$ . When  $\nu$  moles of working fluid pass through a full storage/generation cycle, an amount of heat  $Q_{store} = \nu c_p (T_0^{+(gen)} - T_0^{+(store)})$  must be sloughed off into the environment. This leads to Eqn. (30).

lose any energy but simply degrades it into heat that can be used for other things. For example, the rejection temperature  $T_0^{+(gen)} = 356^\circ\text{K}$ , ( $82^\circ\text{C}$ ) implicit in Fig. 13 is appropriate for making hot water. Cooling towers, such as are required for steam plants, are unnecessary in this case because there is no need to make a Rankine vacuum.<sup>21</sup> Simple thermal cooling ponds will do.

#### E. 19th Century Science

Insofar as the numbers I have presented in this paper are correct, they demonstrate that energy storage is a problem of 19th century science. No laboratory breakthroughs or discoveries are required for solving it. All that is needed is fine engineering and assiduous attention to detail.

Moreover, it is clear from Fig. 11 that storage capacity of months becomes feasible once the engine (including the heat exchangers) exists as a product one can purchase at known cost, particularly if the heat is further transferred to cheaper media for longer-term storage, such as rocks underground. Thus pumped thermal storage with heat exchange is not a niche solution to the energy storage problem but a global one. This is the reason I think it will prevail.

## Acknowledgments

I wish to thank P. Larochele, N. Cizek, J. Kesseli, T. Wolf, R. Apte and T. Geballe for helpful discussions.

- 
- \* R. B. Laughlin: <http://large.stanford.edu>
- <sup>1</sup> D. Lindley, "Smart Grids: The Energy Storage Problem," *Nature* **463**, 18 (2010).
  - <sup>2</sup> R. M. Dell and D. A. J. Rand, "Energy Storage—a Key Technology for Global Energy Sustainability," *J. Power Sources* **100**, 2 (2001).
  - <sup>3</sup> Z. Luo, J. Wang, M. Dooner, and J. Clarke, "Overview of Current Development in Electrical Energy Storage Technologies and the Application Potential in Power System Operation," *Appl. Energy* **137**, 511 (2015).
  - <sup>4</sup> M. Carbajales-Dale, C. J. Barnhart, and S. M. Benson, "Can we Afford Storage? A Dynamic Net Energy Analysis of Renewable Electricity Generation Supported by Energy Storage," *Energy Environ. Sci.* **7**, 1538 (2014).
  - <sup>5</sup> D. Weissbach., G. Ruprecht, A. Huke, K. Czernski, S. Gottlieb, and A. Hussein, "Energy Intensities, EROIs (Energy Return on Invested), and Energy Payback Times of Electricity Generating Power Plants," *Energy* **52**, 210 (2013).
  - <sup>6</sup> E. Hittinger and R. Lueken, "Is Inexpensive Natural Gas Hindering the Grid Energy Storage Industry?" *Energy Policy* **87**, 140 (2015).
  - <sup>7</sup> G. Locatelli, E. Palerma, and M. Mancini, "Assessing the Economics of Large Energy Storage Plants With an Optimisation Methodology," *Energy* **83**, 15 (2015).
  - <sup>8</sup> P. Denholm and M. Hand, "Grid Flexibility and Storage Required to Achieve Very High Penetration of Variable Renewable Energy," *Energy Policy* **39**, 1817 (2011).
  - <sup>9</sup> L. E. Jones, Ed. *Renewable Energy Integration* (Academic press, New York, 2014).
  - <sup>10</sup> G. Swindle, *Valuation and Risk Management in Energy Markets* (Cambridge University Press, Cambridge, 2014).
  - <sup>11</sup> E. Barbour, G. Wilson, P. Hall and J. Radcliffe, "Can Negative Electricity Prices Encourage Inefficient Electrical Storage Devices?" *Int. J. Env. Studies* **71**, 862 (2014).
  - <sup>12</sup> D. Droste-Franke. *Balancing Renewable Energy* (Springer Verlag, Heidelberg, 2012).
  - <sup>13</sup> J. Howes, "Concept and Development of a Pumped Heat Electricity Storage Device," *Proc. IEEE* **100**, 493 (2011).
  - <sup>14</sup> T. Desrues, J. Ruer, P. Marty and J. F. Fourmogu e, "A Thermal Energy Storage Process for Large Scale Electric Applications," *Appl. Therm. Eng.* **30**, 425 (2010).
  - <sup>15</sup> C. P erilhon, S. Lacour, P. Podevin, and G. Descombes, "Thermal Electricity Storage by a Thermodynamic Process: Study of Temperature Impact on the Machines," *Energy Procedia* **36**, 923 (2013).
  - <sup>16</sup> A. Thess, "Thermodynamic Efficiency of Pumped Heat Electricity Storage," *Phys. Rev. Lett.* **111**, 110602 (2013).
  - <sup>17</sup> A. White, G. Parks, and C. N. Markides, "Thermodynamic Analysis of Pumped Thermal Electricity Storage," *Appl. Therm. Eng.* **53**, 291 (2013).
  - <sup>18</sup> *Real Prospects for Energy Efficiency in the United States* (National Academies Press, Washington DC, 2010), p. 280.
  - <sup>19</sup> R. L. Garwin and G. Charpak, *Megawatts and Megatons* (Univ. of Chicago Press, Chicago, 2002).
  - <sup>20</sup> S. A. Wright, R. F. Radel, M. E. Vernon, G. E. Rochau, and P. S. Pickard, "Operation and Analysis of a Supercritical CO<sub>2</sub> Brayton Cycle," Sandia National Laboratories, SAND2010-0171, September 2010.
  - <sup>21</sup> A. S. Leyzerovich, *Steam Turbines for Modern Fossil Fuel Power Plants* (CRC Press, Boca Raton, FL, 2007).
  - <sup>22</sup> *2007 Boiler and Pressure Vessel Code (with Addenda for 2008)* (ASME, New York, 2007), Part II, Section D, Subpart 1, Tables 1A and 1B.
  - <sup>23</sup> H. M uller-Steinhagen, "Concentrating Thermal Power," *Phil. Trans. R. Soc. A* **371**, 20110433 (2013).
  - <sup>24</sup> R. W. Bradshaw and N. P. Siegel, "Molten Nitrate Salt Development for Thermal Energy Storage in Parabolic Trough Solar Power Systems," Sandia National Laboratory, ES2008-54174, August 2008.
  - <sup>25</sup> T. Bauer, D. Liang, and R. Tamme, "Recent Progress in Alkali Nitrate/Nitrite Developments for Solar Thermal Power Applications," in *Molten Salts Chemistry and Technology*, ed by M. Gaune-Escard and G. M. Haarberg (Wiley, 2014).
  - <sup>26</sup> D. J. Rogers and G. J. Janz, "Melting-Crystallization and Premelting Properties of NaNO<sub>3</sub>-KNO<sub>3</sub> Enthalpies and Heat Capacities," *J. Chem. Eng. Data* **27**, 424 (1982).
  - <sup>27</sup> C. M. Kramer and C. J. Wilson, "The Phase Diagram of NaNO<sub>3</sub>-KNO<sub>3</sub>," *Thermochim. Acta* **42**, 253 (1980).
  - <sup>28</sup> X. Zhang *et al.*, "Thermodynamic Evaluation of Phase Equilibria in NaNO<sub>3</sub>-KNO<sub>3</sub> System," *J. Phase Equil. and Diffusion* **24**, 441 (2003).
  - <sup>29</sup> D. A. Nissen and D. E. Meeker, "Nitrate/Nitrite Chemistry in NaNO<sub>3</sub>-KNO<sub>3</sub> Melts," *Inorg. Chem.* **22**, 716 (1983).
  - <sup>30</sup> E. S. Freeman, "The Kinetics of the Thermal Decomposition of Potassium Nitrate and of the Reaction Between Potassium Nitrite and Oxygen," *J. Am. Chem. Soc.* **79**, 838 (1957).
  - <sup>31</sup> P. Gimenez and S. Fereres, "Effect of Heating Rates and Composition on the Thermal Decomposition of Nitrate Based Molten Salts," *Energy Procedia* **69**, 654 (2013).
  - <sup>32</sup> R. I. Olivares, "The Thermal Stability of Molten Nitrite/Nitrates Salt for Solar Thermal Energy Storage in Different Atmospheres," *Solar Energy* **86**, 2576 (2012).
  - <sup>33</sup> S. H. Goods and R. W. Bradshaw, "Corrosion of Stainless Steels and Carbon Steel by Molten Mixtures of Commercial Nitrate Salts," *J. Mater. Eng. Perform.* **13**, 78 (2004).
  - <sup>34</sup> A. Kruiuzenga and D. Gill, "Corrosion of Iron Stainless Steels in Molten Nitrate Salt," *Energy Procedia* **49**, 878 (2014).
  - <sup>35</sup> G. L. Janz, U. Krebs, H. F. Siegenthaler, and R. P. T. Tomkins, "Molten Salts: Volume 3, Nitrates, Nitrites, and Mixtures," *J. Phys. Chem. Ref. Data* **1**, 581 (1972).
  - <sup>36</sup> M. Lasfargues, H. Cao, Q. Geng, and Y. Ding, "Rheological Analysis of Binary Eutectic Mixture of Sodium and Potassium Nitrate and the Effect of Low Concentration CuO Nanoparticle Addition to Its Viscosity," *Materials* **8**, 5194 (2015).

- <sup>37</sup> T. Bauer, N. Pflieger, N. Breidenbach, M. Eck, D. Liang, and S. Kaesche, "Material Aspects of Solar Salt for Sensible Heat Storage," *Appl. Energy* **111**, 1114 (2013).
- <sup>38</sup> "Toxicological Profile for *n*-Hexane," U.S. Department of Health and Human Services, July 1999.
- <sup>39</sup> P. Arlien-Søborgs, *Solvent Neurotoxicity* (CRC Press, 1991).
- <sup>40</sup> E. J. Conkerton, P. J. Wan, and O. A. Richard, "Hexane and Heptane as Extraction Solvents for Cottonseed: A Laboratory-Scale Study," *J. Am. Oil Chem. Soc.* **72**, 963 (1995).
- <sup>41</sup> H. Dominguez, M. J. Nuñez, and J. M. Lema, "Enzyme-Assisted Hexane Extraction of Soya Bean Oil," *Food Chem.* **54**, 223 (1995).
- <sup>42</sup> A. Rosenthal, D. L. Pyle, and K. Niranjana, "Aqueous and Enzymatic Processes for Edible Oil Extraction," *Enzyme Microb. Tech.* **19**, 402 (1996).
- <sup>43</sup> T. W. Yergovich, G. W. Swift, and F. Kurata, "Density and Viscosity of Aqueous Solutions of Methanol and Acetone from the Freezing Point to 10 °C," *J. Chem. Eng. Data* **16**, 222 (1971).
- <sup>44</sup> F. A. M. Gonçalves, A. R. Trindade, C. S. M. F. Costa, J. C. S. Bernardo, and I. Johnson, "PVT, Viscosity, and Surface Tension of Ethanol: New Measurements and Literature Data Evaluation," *J. Chem. Thermodynamics* **42**, 1039 (2010).
- <sup>45</sup> C. W. Kanolt, "Nonflammable Liquids for Cryostats," *Scientific Papers of the Bureau of Standards* **60**, 619 (1925).
- <sup>46</sup> R. Hossaini, M. P. Chipperfield, S. A. Montzka, A. Rap, S. Dhomse, and W. Fang, "Efficiency of Short-Lived Halogens at Influencing Climate Through Depletion of Stratospheric Ozone," *Nature Geosci.* **8**, 186 (2015).
- <sup>47</sup> V. P. Brykov, G. Kh. Mukhamedzyanov, and A. G. Usmanov, "Experimental Investigation of the Thermal Conductivity of Organic Fluids at Low Temperatures," *J. End. Phys.* **18**, 62 (1070) [*Inzhen.-Fiz. Zh.* **18**, 82 (1970)].
- <sup>48</sup> M. J. Assael, E. Charitidou, C. A. Nieto de Castro, and W. A. Wakeman, "The Thermal Conductivity of *n*-Hexane, *n*-Heptane, and *n*-Decane by the Transient Hot-Wire Method," *Int. J. Thermophys.* **8**, 663 (1987).
- <sup>49</sup> E. B. Giller and H. G. Drickamer, "Viscosity of Normal Paraffins Near the Freezing Point," *Ind. Eng. Chem.* **41**, 2067 (1949).
- <sup>50</sup> B. Knapstad, P. A. Skjøisik, and H. A. Øye, "Viscosity of Pure Hydrocarbons," *J. Chem. Eng. Data* **34**, 37 (1989).
- <sup>51</sup> B. Kalinowska, J. Jelińska, W. Wóycicki, and J. Stecki, "Heat Capacities of Liquids at Temperatures Between 90 and 300 K and at Atmospheric Pressure I. Method and Apparatus, and the Heat Capacities of *n*-Heptane, *n*-Hexane, and *n*-Propanol," *J. Chem. Thermodyn.* **12**, 891 (1980).
- <sup>52</sup> H. Crauber, "Densitometer for Absolute Measurements of the Temperature Dependence of Density, Partial Volumes, and the Thermal Expansivity of Solids and Liquids," *Rev. Sci. Instrum.* **57**, 2817 (1986).
- <sup>53</sup> E. W. Lemmon, M. O. McLinden and D. G. Friend, "Thermophysical Properties of Fluid Systems," in *NIST Chemistry Webbook, NIST Standard Reference Database Number 69*, ed. by P. J. Linstrom and W. G. Mallard, U.S. National Institute of Standards and Technology, January 2013.
- <sup>54</sup> S. K. Roberts and S. A. Sjolander, "Effect of the Specific Heat Ratio on the Aerodynamic Performance of Turbomachinery," *J. Eng. Gas Turbines Power* **127**, 773 (2002).
- <sup>55</sup> F. P. Incropera and D. P. DeWitt, *Fundamentals of Heat and mass Transfer* (Wiley, 2006).
- <sup>56</sup> B. J. Mckeon, C. J. Swanson, M. V. Zagarola, R. J. Donnelly, and A. J. Smits, "Friction Factors for Smooth Pipe Flow," *J. Fluid Mech.* **511**, 41 (2004).
- <sup>57</sup> K. Huang, *Statistical Mechanics* (Wiley, 1963), p. 107.
- <sup>58</sup> D. Beck and D. G. Wilson, *Gas Turbine Regenerators* (Springer, 2011).
- <sup>59</sup> L. H. Smith, "Axial Compressor Aerodesign Evolution at General Electric," *J. Turbomach.* **124**, 321 (2002).
- <sup>60</sup> A. R. Wadia, D. P. Wolf, and F. G. Haaser, "Aerodynamic Design and Testing of an Axial Flow Compressor with Pressure Ratio of 23:3:1 for the LM2500+ Gas Turbine," *J. Turbomach.* **124**, 331 (2002).
- <sup>61</sup> A. F. El-Sayed, *Aircraft Propulsion and Gas Turbine Engines* (CRC Press, 2008), p. 273.
- <sup>62</sup> D. Eckhardt, *Gas Turbine Powerhouse, 2nd Ed.* (Oldenbourg Wissenschaftsverlag, 2014), p. 152.
- <sup>63</sup> J. K. Schweitzer and J. D. Smith, "Advanced Industrial Gas Turbine Technology Readiness Demonstration Program: Phase II Final Report, Compressor Rig Fabrication, Assembly and Test," U.S. Department of Energy, DOE/OR/05035-T2, March 1981.
- <sup>64</sup> D. K. Hall, E. M. Greitzer, and C. S. Tan, "Performance Limits of Axial Turbomachine Stages," in *Proc. ASME Turbo Expo*, Vol. 8, Part A, p. 479 (ASME, 2012).
- <sup>65</sup> J.-M. Tournier and M. S. El-Genk, "Axial Flow, Multi-Stage Turbine and Compressor Models," *Energy Convers. Manage.* **51**, 16 (2010).
- <sup>66</sup> M. P. Boyce, *Gas Turbine Engineering Handbook, 4th Ed.* (Butterworth-Heinemann, 2011).
- <sup>67</sup> L. M. Larosiliere, J. R. Wood, M. D. Hathaway, A. J. Medd, and T. Q. Dang, "Aerodynamic Design Study of Advanced Multistage Axial Compressor," National Aeronautics and Space Administration, NASA/TP-2002-211568, December 2002.
- <sup>68</sup> *ASME Code for Pressure Piping, B31: an American National Standard* (ASME, 2008).
- <sup>69</sup> "Standard Specification for Seamless Carbon Steel Pipe for High Temperature Service," American Society for Testing and Materials, ASME A 106/A 106M - 06a, October 2006, paragraph 16-3.
- <sup>70</sup> A. Aquaro and M. Pieve, "High Temperature Heat Exchangers for Power Plants: Performance and Advanced Metallic Recuperators," *Appl. Therm. Eng.* **27**, 389 (2007).
- <sup>71</sup> N. Tsuzuki, Y. Kato, and T. Ishiduka, "High Performance Printed Circuit Heat Exchangers," *Appl. Therm. Eng.* **27**, 1702 (2007).
- <sup>72</sup> F. J. Brooks, "GE Gas Turbine Performance Characteristics," GE Power Systems, GER-3567H, October 2000.
- <sup>73</sup> "Cost and Performance Data for Power Generation Technologies," Black and Veach, prepared for the U.S. National Renewable Energy Laboratory, February 2012.
- <sup>74</sup> R. Tidball, J. Bluestein, N. Rodriguez, and S. Knoke, "Cost and Performance Assumptions for Modeling Electricity Generation Technologies," U.S. National Renewable Energy Laboratory, NREL/SR-6A20-48595, November 2010.
- <sup>75</sup> M. D. Fenton, "Iron and Steel," U.S. Geological Survey Minerals Yearbook, October 2015.
- <sup>76</sup> L. E. Apodaca, "Nitrogen", U.S. Geological Survey Minerals Handbook, August 2015.

- <sup>77</sup> “Petroleum Marketing Monthly,” U.S. Energy Information Administration, January 2016.
- <sup>78</sup> H. P. Loh, J. Lyons and C. W. White III, “Process Equipment Cost Estimation: Final Report,” U.S. DOE/NETL-2002/1169, January 2002.
- <sup>79</sup> “Welded Steel Tanks for Oil Storage,” Am. Petrol Inst., API Standard 650, February 2012.
- <sup>80</sup> B. Christensen, “Cost Estimating guide for Road Construction,” U.S. Forest Service Northern Region Engineering, February 2011.
- <sup>81</sup> Task Committee on Pumped Storage of the Hydropower Committee of the energy Division of the American Society of Civil Engineers, *Compendium of Pumped Storage Plants in the United States* (ASCE, 1993).
- <sup>82</sup> B. Dunn, H. Kamath, and J.-M. Tarascon, “Electrical Energy Storage for the Grid: A Battery of Choices,” *Science* **334**, 928 (2011).
- <sup>83</sup> D. Rastler, “Electricity Energy Storage: Technology Options,” Electric Power Research Institute, Report 1020676, December 2010.
- <sup>84</sup> J. P. Deane, B. P. O. Gallachóir, and E. J. McKeogh, “Techno-Economic Review of Existing and New Pumped Hydro Energy Storage Plant,” *Renew. Sustain. Energy Rev.* **14**, 1293 (2010).
- <sup>85</sup> S. Rahman, L. M. Al-Hadhrami, and Md. M. Alam, “Pumped Hydro Energy Storage System: A Technological Review,” *Renew. Sustain. Energy Rev.* **44**, 586 (2015).
- <sup>86</sup> T. Reddy, *Linden’s Handbook of Batteries, 4th Ed.* (McGraw-Hill, 2010).
- <sup>87</sup> K. E. Aifantis, S. A. Hackney, and R. V. Kumar, “High Energy Density Lithium Batteries: Materials, Engineering, Applications,” (Wiley-VCH, 2010), p. 72.
- <sup>88</sup> R. Van Noorden, “A Better Battery,” *Nature* **507**, 294 (2014).
- <sup>89</sup> E. M. Krieger, J. Cannarella, and C. B. Arnold, “A Comparison of Lead-Acid and Lithium-Based Battery Behavior and Capacity Fade in Off-Grid Renewable Charging Applications,” *Energy* **60**, 492 (2013).
- <sup>90</sup> G. I. Soloveichik, “Flow Batteries: Current Status and Trends,” *Chem. Rev.* **115**, 11533 (2015).
- <sup>91</sup> A. Z. Weber, M. M. Mench, J. P. Meyers, P. N. Ross, J. R. Gostick, and Q. Liu, “Redox Flow Batteries: A Review,” *J. Appl. Electrochem.* **41**, 1137 (2011).
- <sup>92</sup> K. Gong, X. Ma, K. M. Conforti, K. J. Juttler, J. B. Grunewald, K. L. Yeager, M. Z. Bazant, S. Gu and Y. Yan, “A Zinc-Iron Redox-Flow Battery Under \$100 per kWh of System Capital Cost,” *Energy Environ. Sci.* **8**, 23941 (2015).
- <sup>93</sup> H. Kim, D. A. Boysen, J. M. Newhouse, B. L. Spatocco, B. Chung, P. J. Burke, D. J. Bradwell, K. Jiant, A. A. Tomaszowska, K. Want, W. Wei, L. A. Ortiz, S. A. Barriga, S. M. Poizeau, and D. R. Sadoway, “Liquid Metal Batteries: Past, Present and Future,” *Chem. Rev.* **113**, 2075 (2013).
- <sup>94</sup> D. I. Wood III, J. Li and C. Daniel, “Prospects for Reducing the Processing Cost of Lithium Ion Batteries,” *J. Power Sources* **275**, 234 (2015).
- <sup>95</sup> G. Pistoia, J.-P. Wiaux, and S. P. Wolsky, *Used Battery Collection and Recycling* (Elsevier, 2001).
- <sup>96</sup> G. W. Richter and K. Solez, Eds., *International Review of Experimental Pathology: Transition Metal Toxicity (Vol. 31)* (Academic Press, 1990).
- <sup>97</sup> C. J. Rydh, “Environmental Assessment of Vanadium Redox and Lead-Acid Batteries for Stationary Energy Storage,” *J. Power Sources* **80**, 21 (1999).
- <sup>98</sup> G. Majeau-Bettez, T. R. Hawkins, and A. H. Stromman, “Life Cycle Environmental Assessment of Lithium-Ion and Nickel Metal Hydride Batteries for Plug-In Hybrid and Battery Electric Vehicles,” *Environ. Sci. Technol.* **45**, 4548 (2011).
- <sup>99</sup> D. A. Notter, M. Grauch, R. Widmer, P. Wäger, A. Stamp, R. Zah and A.-J. Althaus, “Contribution of Li-Ion Batteries to the Environmental Impact of Electric Vehicles,” *Environ. Sci. Technol.* **44**, 6550 (2010).
- <sup>100</sup> G. Saur and T. Ramsden, “Wind Electrolysis: Hydrogen Cost Optimization,” U.S. National Renewable Energy Laboratory, NREL/TP-5600-50408, May 2011.
- <sup>101</sup> P. W. Parfomak, “Energy Storage for Power Grids and Electric Transportation: A Technology Assessment,” Congressional Research Service, CRS Report for Congress R42455, March 2012.
- <sup>102</sup> A. A. Akhil, G. Huff, A. B. Currier, B. C. Kaun, D. M. Rastler, S. B. Chen, A. L. Cotter, D. T. Bradshaw, and W. T. Gauntless, “DOE/EPRI Electricity Storage Handbook in Collaboration with NRECA,” Sandia National Laboratory, SAND2013-5131, February 2015.
- <sup>103</sup> F. S. Barnes and J. G. Levine, *Large Energy Storage Systems Handbook* (CRC Press, 2011), p. 111.
- <sup>104</sup> J. O. Goodson, “History of First U.S. Compressed Air Energy Storage (CAES) Plant,” Electric Power Research Institute, EPRI TR-101751, December 1992.
- <sup>105</sup> G. Grazzini and A. Milazzo, “A Thermodynamic Analysis of Multistage Adiabatic CAES,” *Proc. IEEE* **100**, 461 (2012).
- <sup>106</sup> E. Barbour, D. Mignard, Y. Ding, and Y. Li, “Adiabatic Compressed Air Energy Storage With Packed Bed Thermal Energy Storage,” *Appl. Energy* **155**, 804 (2015).
- <sup>107</sup> W. Liu, L. Liu, L. Zhou, J. Huang, U. Zhang, G. Xu, and Y. Yang, “Analysis and Optimization of a Compressed Air Energy Storage-Combined Cycle,” *Entropy* **16**, 3103 (2014).
- <sup>108</sup> B. P. McGrail, C. L. Davidson, D. H. Bacon, M. A. Chamness, S. P. Reigel, F. A. Spane, J. E. Cabe, F. S. Knudsen, M. D. Bearden, J. A. Horner, H. T. Schaeff, and P. D. Thorne, “Techno-Economic Performance Evaluation of Compressed Air Energy Storage in the Pacific Northwest,” Pacific Northwest Laboratory, PNNL-22235, February 2013.
- <sup>109</sup> H. Safaei, D. W. Keith, and R. J. Hugo, “Compressed Air Energy Storage (CAES) with Compressors Distributed at Heat Loads to Enable Waste Heat Utilization,” *Appl. Energy* **103**, 165 (2013).
- <sup>110</sup> “Case Study: Heat Exchanger Rupture and Ammonia Release in Houston, Texas,” U.S. Chemical Safety and Hazard Investigation Board, 2008-06-I-TX, June 2008.
- <sup>111</sup> R. X. Faivre Pierret, P. Berne, C. Roussel, and F. Le Guern, “The Lake Nyos Disaster: Model Calculations for the Flow of Carbon Dioxide,” *J. Vulcanol. Geotherm. Res.* **51**, 161 (1992).